ICAS 2020 SHANGHAI
International Council of the Aeronautical Sciences
32nd Congress of the International Council of the Aeronautical Sciences
September 6-10, 2021
Pudong Shangri-La, Shanghai, China

HYBRID IGNITION PROBABILITY METHOD TO PREDICT THE IGNITION PERFORMANCE OF A GAS TURBINE COMBUSTOR

Xiao Wei[1], Cheng Yajun[2], Wang Ke[3], Ren Zhuyin[4]
[1]AECC Hunan Aviation Powerplant Research Institute, Zhuzhou, China
[2]HUNAN MECHANICAL & ELECTRICAL POLYTECHNIC, Changsha, China
[3]Aero Engine Academy of China (AECC), Beijing, China
[4]Institute for AeroEngine, Tsinghua University

Abstract

Ignition and high-altitude reignition in the aeroengine are critical issues in the design stage of gas turbine combustor. The tools for ignition performance optimization and prediction are hence needed and are the objective of this contribution. In present study, ignition process inside a rich-burn gas turbine combustor is investigated numerically by a hybrid ignition probability analysis method, in which the ignition probability is predicted by the kernel formation criteria coupled with flame particle tracking method. The in-house code, which has been validated for the bluff-body flame, is applied to adjust for a gas turbine combustor. This code is based on the criteria for the successful ignition process, which starts with the first flame kernel formation in the combustor. For the first kernel formation, the effect of turbulent scalar transport on flammability is modeled through the incorporation of turbulence-induced diffusion in a spherically outwardly propagating flame kernel model. For the flame propagation, the Lagrangian flame particle tracking method is used and the Karlovitz number is employed for extinction criterion. In comparison with ignition data from the combustor, the code's results show good agreements, indicating that the local kernel formation criteria coupled with the flame particle tracking method can be used to optimize and predict the ignition performance.

Keywords: Ignition probability, kernel formation, flame particle, gas turbine combustor

1. Introduction

The ignition performance in the gas turbine combustor is one of the most important aspects for aeronautical engines. The ignition phenomenon can be classified into two types: forced ignition and autoignition. The forced ignition that induced by an electrical spark or a plasma jet is commonly used in the gas turbine combustor. The evaluation of spark ignition performance with reasonable accuracy is an essential requirement of combustor design activity. However, ignition is a complex transient phenomenon, not yet fully understood and controlled [1]. Such phenomena pose challenges for both empirical and analytical modeling works of practical combustors because combustion occurs mostly at the smallest and unresolved scales.

With the need to be able to optimize and predict the ignition performance, many experimental and theoretical studies have been conducted since 1970s [2-4]. Lefebvre and coworkers [5-7] reported a series of experimental-analytical studies, dealing with the spark ignition of gaseous and spray mixtures. Peters and Mellor also [8-10] developed a characteristic time model that yielded the ignition limits as a function of turbulent mixing time, kinetic time, and evaporation time. These models are highly dependent on the empirical constant which is usually obtained from the experiments. These experiments are expensive and time-consuming because of hardware manufacturing and high-altitude conditions required for the test. Large eddy simulations (LES) seem ideal for capturing spark ignition [11-14]. But LES can only be performed on the high-performance computers and the computing time may exceed the time frame for engine development projects.

An alternative modeling strategy is to use low-order, physics-based models coupled with cold flow CFD simulation, which is much cheaper in term of costs and time. This approach is very useful for engine developers because they can provide quick answers on the ignition behavior of a combustor. Eyssartier [15-16] focused on the flame kernel formation and derived a local ignition criterion, giving the probability of ignition from the knowledge of the unsteady non-reacting two-phase flow. Neophytou [17] focused on the flame expansion process and proposed an ignition probability analysis approach, in which a Lagrangian particle tracking method is employed for flame propagation and stabilization. However, these efforts are insufficient to capture the ignition sequences because a complete ignition process includes both kernel formation process and flame propagation process.

In order to improve the prediction accuracy of spark ignition, the Lagrangian particle tracking method coupled with local ignition criteria for kernel formation has been integrated into the ignition code, which is developed from Tsinghua University and AECC. This code for modeling of ignition process relies on the cold flow simulation on spray mixtures, and has been validated for a bluff-body flame. With the needs to optimize and predict the ignition performance in the practical combustor, the code has been further validated with the experimental data of a model combustor from AECC in present study.

2. Experimental methodology

2.1 Apparatus

Ignition experiment was conducted using high-altitude ignition test system at HAPRI, Zhuzhou, China. The test rig is showed in Fig.1. A single dome combustor with optical access was mounted inside a pressure vessel. This combustor was designed with an inclination angle to match the air flow delivered by the centrifugal compressor, which is commonly used in small engines. The radial diffuser was assembled together with the combustor to simulate the air flow departed from the centrifugal compressor in the practical engine. In order to separate the upper and lower flow passages and simulate the actual pressure distribution of the full annular combustor, there was no gas between the combustor and liner sidewall. In addition, quartz windows of 87mm*141mm were installed on the sidewalls of casing and liner to facilitate visualization of the ignition events using high-speed camera.

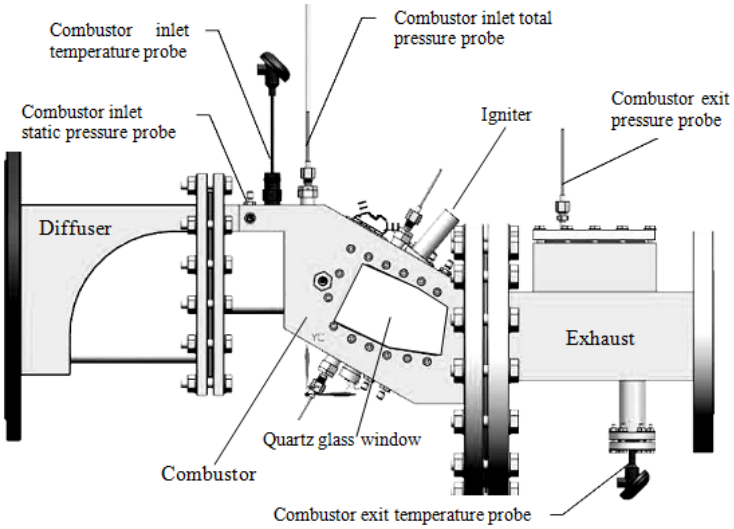

Figure 1 Schematic of test rig

The injection system consists of a radial swirler and two axial swirlers with a dual-orifice atomizer nested in the center. The RP-3 kerosene was supplied in controlled quantities via a mass flow controller. A refrigeration unit and vacuum pump located upstream and downstream of the combustor allowed independent control of air temperature, pressure, and mass flow rate inside the combustion chamber.

The sparks were generated by two electric spark igniters with constant spark energy of 6J. The igniter was located upstream of primary holes with 5 degree angle to the injector midplane. The igniter tip was assembled flush with the combustor liner wall to avoid the interference of flow distribution in the combustor chamber. In the experiment, the spark energy was discharged at a

frequency of 1.2Hz. Therefore the spark was generated every 833 ms until the test was terminated. The experimental setups for ignition in the combustors are shown in Table 1.

2.2 Diagnostics

In the experiment process, the fuel path was connected to the pilot nozzle of the atomizer. After setting the fuel air ratio (FAR) to the desired condition, the solenoid valve was switched to supply fuel to the fuel nozzle inside the combustor and the igniter was turned on. The igniter continues until ignition or no ignition in 10 seconds. The measured combustion chamber outlet temperature was used to determine the ignition success point. Once the exit temperature of the combustion chamber begins to soar, this indicates a successful ignition event (see Figure 2). The interval between the tests is 3–5 minutes. Continuous air supply was used during the interval to ensure that the residual fuel inside the liner is blown away. At a given pressure drop, the minimum FAR leading to successful ignition, which was identified from the data of ignition success points and ignition failure points, was regarded as the lean ignition boundary. A high-speed camera, Photron FASTCAM SA4, was used in ignition visualization experiments, in conjunction with the AF-S Micro NIKKOR Glens. A typical graph of ignition process is illustrated in Figure 3.

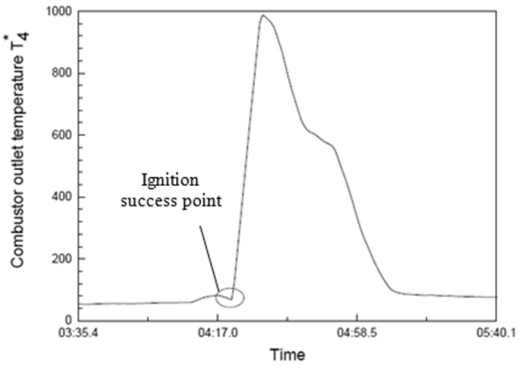

Figure 2 Successful ignition event

Figure 3 Successful ignition sequence

2.3 Operating Conditions

Ignition testing was conducted at both high-altitude and ambient operating conditions, and test operating conditions (TOC) were listed in Table1. Flow parameters have been defined to facilitate the analysis of the combustor flow characteristics in the experiments. These parameters include the residence time and reference velocity, which is mean velocity across the plane of maximum cross-sectional area of the combustor. This reference velocity can be written as

$$U_r = \frac{m_a}{\rho_a A_r} \tag{1}$$

The residence time is equal to the ratio of the air mass which occupies the volume of combustor, divided by the air mass flow. This residence time can be written as

$$\tau_{residence} = \frac{\rho_a V_C}{m_a} \tag{2}$$

Table 1 Test operating conditions of spark ignition

TOC	P_3, kPa	T_3, K	U_r, m/s	τ, ms
1	100.7	288	5.3	29
2	102.2	288	7.8	20
3	101.5	288	9.4	16
4	102.6	288	10.8	14
5	104.5	288	12.2	12

3. Numerical setup

The use of ignition code requires the results of cold flow simulation as input of the code. Therefore, Validations for both ignition model and CFD simulation are needed before implementing the hybrid ignition probability method.

3.1 Cold Flow CFD Simulation

CFD simulations are conducted on the two phase non-reaction flow. In the implementation of the CFD simulation, the combustor is meshed with an unstructured grid of 21 million cells. The turbulence is solved with the realizable $k-\varepsilon$ model. The realizable $k-\varepsilon$ model has been used extensively in the solution of swirling flow. A remarkable advantage of the realizable $k-\varepsilon$ model is to accurately predict the flows involving rotation, boundary layers under strong adverse pressure gradients, separation and recirculation.

The spray model is of great importance for the mixture fraction distribution, which plays a significant role on the flame kernel formation and propagation. In present study, the primary breakup model is simplified and represented by a cone spary with Rosin-Rammler distribution [18] at the nozzle exit. The Rosin-Rammler distribution can be written as

$$V = 1 - exp\left[-\left(\frac{d}{d_n}\right)^n\right] \tag{3}$$

Here, n is the spread exponent, d_n is the droplet diameter such that 63.2% of the total liquid volume is in drops of smaller diameter. Rizk [19] proposed a correlation between d_n and Sauter mean diameter (SMD), it gives

$$d_n = (0.91SMD)^{1.18} \tag{4}$$

In present study, the Sauter mean diameter and spread exponent are measured from the experiment and used as input of the Rosin-Rammler distribution. As the droplets transport towards to the downstream, the SSD model is employed as the secondary breakup model to capture the atomization process. The secondary breakup occurs when the drop size exceed the critical radius, which can be expressed as

$$R_{critical} = \frac{\sigma_1 We_{cr}}{\rho_a U_{rel}^2} \tag{5}$$

where σ_1 is the surface tension, We_{cr} is the critical Weber number, U_{rel} is the relative velocity.

The two phase flow model consists of a fully coupled combination of Lagrangian droplet and Eulerian fluid calculations, and the motion of each droplet is solved by the equations given by

$$\frac{dV}{dt} = \frac{U_i - V_i}{\tau_d} + g \tag{6}$$

where U_i is the gas velocity, V_i is the drop velocity, τ_d is the characteristic time, g is the additional acceleration term.

3.2 Ignition model description

The main idea of the code is to capture the initial flame kernel formed by spark energy and track the flame kernel from the ignition site towards to the injector and central recirculation zone. Hence, the ignition code can be mainly divided into two parts, which are programed to describe the initial kernel formation and flame propagation, respectively. The ignition model is based on the following steps:

1) Formation of a sustainable flame kernel

Firstly, the fuel is injected into the combustor chamber and forms a flammable mixture. Subsequently, the ignition triggered by a spark and leads to the creation of a small hot gas kernel with the temperature required for ignition. The formation of the first flame kernel then would be

induced by the high temperature of the hot gas kernel. However, this flame kernel can be sustainable only when the vaporization time of droplet is small compared to the quench time. As all of these requirements are met, the initial flame kernel is able to grow in size and propagate towards to the injector. Thus, three criteria are required for the initiation of a sustainable flame kernel. The first one is that the equivalence ratio must be within the flammability limits,

$$\phi_{low} \leq \phi \leq \phi_{high} \tag{7}$$

where ϕ_{low} and ϕ_{high} are the low and high flammability limits respectively and they are in general flow dependent.

The second criterion is that the energy deposit E must at least increase the unburnt mixture temperature T_∞ of gas mixture to its ignition temperature T_{ign} and bring the temperature of cold liquid fuel T_f to its saturation temperatureT_{cc},

$$\frac{E}{\rho C_p} \geq \left(T_{ign} - T_\infty\right) + \frac{\rho_l C_{p,l}}{\rho C_p}\left(\alpha_l + \frac{4n_{dim}}{3Nu}\frac{d_l^2}{d_k^2}\right)\left(T_{cc} - T_f\right) \tag{8}$$

where α_l is the volume fraction of liquid, n_{dim} is the number of space dimensions, Nu is the Nusselt number, d_k is the size of flame kernel, d_l is the diameter of fuel droplet, ρ and ρ_l are the gas density and liquid density respectively, C_p and $C_{p,l}$ are the specific heat of gas and liquid, respectively. The ignition temperature T_{ign} of the liquid fuel can be expressed as a function of the equivalence ratio.

The third criterion, which is originally proposed by Ballal and Lefebvre [20], is that the time required for evaporation and burning must be less than or equal to the time required for the cold surrounding mixture to quench the spark kernel, i.e.,

$$\tau_{vap} + \tau_{comb} \leq \tau_q \tag{9}$$

Here, τ_{vap} is the evaporation time, τ_{comb} is the combustion characteristic time, τ_q is the quench time. As the combustion characteristic time τ_{comb} is much smaller than τ_{vap} and τ_q, and it is equivalent to

$$\frac{d_k}{d_l} \geq \sqrt{\frac{4n_{dim}\rho_l}{3\phi \cdot \mathrm{Sh} \cdot \rho \cdot \mathrm{In}(1+B_m)}} \tag{10}$$

where B_m is the mass Spalding number and Sh is the Sherwood number. This compares the kernel size d_k to the droplet diameter d_l.

With the above three criteria for flame kernel formation, the probability map of kernel formation in turbulent flames can be computed through the following three steps. First, with the mean mixture fraction and its variance being extracted from a non-reacting simulation, a beta probability density distribution function is used to generate many realizations of fuel/air mixtures for each location, which is 100 in this work. Then, the criteria are applied for individual samples at each location of the cold flow. Finally, the percentage of events satisfying the criteria for successful kernel formation is counted to form the probability map of kernel formation.

2) Lagrangian flame particle tracking

With the successful formation of a sustainable flame kernel, the flame is able to propagate towards to the injector and central recirculation zone. During the period of the flame propagation, the flame particles are released from the spark location, and the flame particles are tracked through the following procedures:

i. The flow is filled with structured “grid cells’’. These grid cells can have two states, cold or burnt. Initially, all grid cells are in the cold state. Cells could be placed throughout the CFD domain or only in a selected region. All grid cells that overlap with the spark volume are switched to the burnt state and each of them releases a ‘‘flame particle’’.

ii. The flame particle is tracked with the Langevin model within the cold CFD field being interpolated to the structured grid. The particles have velocity and mixture fraction with mean and random components determined by the CFD solution. At each position during its trajectory, a particle can extinguish according to the criterion based on a Karlovitz number. When a particle extinguishes, it is no longer tracked.

iii. Every time a particle visits a grid cell in a cold state, the grid cell switches to the burnt state and a new particle, with its own random velocity and mixture fraction being sampled from the local velocity and mixture fraction distributions, is emitted at its center and follows its own random

walk. For each ignitor location, once all the active flame particles being tracking, the status of cells, e.g., burnt and unburnt can be summarized.

iv. The ignition progress factor (IPF), π_{Ign}, defined as the fraction of cells in burnt state for a given domain of interest, can be obtain as a function of the time. At the end of the simulation, if the π_{ign} is larger than a critical threshold $\pi_{Ign,crit}$, the ignition of the whole flame is declared to be successful. If not, the ignition of this ignition event is declared to be failed.

v. For each spark location, the above computation is repeated many times with different realizations to obtain the mean ignition progress factor and successful ignition probability, P_{Ign}. By repeating this calculation for different spark locations, maps of mean and variance of ignition progress factor and ignition probability can be created.

The flame particle tracking method is applied to analyze the flame propagation and stabilization process after successful kernel formation. The motion of flame particles is given by

$$dX_{p,i} = U_{p,i}dt \tag{11}$$

$$dU_{p,i} = \left(\frac{1}{2} + \frac{3}{4}\mathrm{C}_0\right)\omega_p\left(U_{p,i} - \widetilde{U_\iota}\right)dt + \left(C_0\varepsilon_p dt\right)^{0.5}N_{p,i} \tag{12}$$

where $X_{p,i}$ is the flame particle location, $U_{p,i}$ is the particle velocity in direction i, $\widetilde{U_\iota}$is the local mean velocity of the flow, $N_{p,i}$ is a normally distributed variable (with mean zero and variance unity), ω_p is turbulence frequency and is related to turbulent kinetic energy k_p and dissipate rate ε_p at the particle location through $\omega_p = \varepsilon_p/k_p$, C_0 is the model constant taken to be 2.

During the period of flame propagation, the flame particle exchanges the mass with the local cell through

$$\frac{dZ_p}{dt} = -0.5C_0\omega\left(z_p - \tilde{z}\right) + (1 - \tilde{z})\frac{\overline{\Gamma_m}}{\bar{\rho}} \tag{13}$$

where z_p is the particle mixture fraction, $\tilde{z}$ is the local mean mixture fraction in the flow, $\bar{\rho}$ is the local density of gaseous mixture, and $\overline{\Gamma_m}$ is the mean evaporation rate from the local CFD cell. Note that Eq. (13) assumes the mass and energy interaction by exchange with the mean of the local CFD cell.

At the end of each time step, a criterion based on a Karlovitz number is used to assess if the flame particle extinguishes. A Karlovitz number Ka_p is defined for each particle and is compared to a critical value$Ka_{p,crit}$. If Ka_p>$Ka_{p,crit}$, the particle extinguishes. As shown Reference [21], the Karlovitz number Ka_p is defined as the ratio between the chemical time and the reciprocal eddy lifetime, i.e.,

$$Ka_p = 0.157\left(\upsilon\frac{\left(u_p'\right)^3}{L_{turb,p}}\right)^{0.5}\frac{1}{S_{L,P}^2} \tag{14}$$

where υ is the mixture kinematic viscosity, $L_{turb,p}$ and u_p' is the turbulence integral length and turbulent fluctuating velocity at the particle location, respectively, and $S_{L,p}$ is the laminar flame speed. Given the particle mixture fraction z_p, the corresponding laminar flame speed is precalculated and then Ka_p is computed via Eq. (14) with the flow information being extracted from a nonreacting simulation.

4. Results and discussion

4.1 Kernel formation probability map

Figure4 shows the kernel formation probability of the central plane in the combustor, and the results are calculated with different FARs under TOC1. It is noted that the minimum FAR for ignition under TOC1 is 0.031 based on the experiment, and the kernel formation probability map with FAR=0.031 is illustrated in Figure4(c). As shown in Figure4(a), high values of kernel formation probability is observed in the primary zone, which indicates excellent ignition ambient with FAR in primary zone exceeds the equivalence ratio. However, Figure4 (b),(c),(d) and (e) show the highlight in the primary zone shrink as FAR decreases. It is evident that the kernel formation probability is deeply dependent on the FAR. This is because the spray atomization quality is improved by increasing FAR. Hence, the initial flame kernel can be generated successfully with meeting the criterion for the flammability and characteristic time. It is also noted that there is a huge difference between the highlight in Figure4(c) and (d). This difference indicates the lean ignition limit is closely linked to the kernel formation probability.

Figure5 illustrates the effect of reference velocity on the kernel formation probability. It is noted that the ignition is failed in Figure5 (a) and successful in Figure5 (b), (c) based on the experimental results. As shown in Figure5, the kernel formation probability increases with the reference velocity. These trends indicate that the beneficial effects on ignition performance can be obtained by increasing the reference velocity. The similar effect of reference velocity on the ignition has been reported in references [22]. This is mainly attributed to the improved atomization resulting from the increased reference velocity. Moreover, it is also worth mentioning that the high kernel formation probability in the shear layer is evident as shown in Figure6 and 8, and this agrees with experimental observations.

The kernel formation probability profiles showed in Figure4 and Figure5 can be used for quickly assessing both igniter position and ignition performance, because the computational expense of these calculations is lower compared with the flame particle tracking. However, the profiles of kernel formation probability are insufficient for predicting the ignition limits, since the propagation of initial flame kernels is also important for the flame stability.

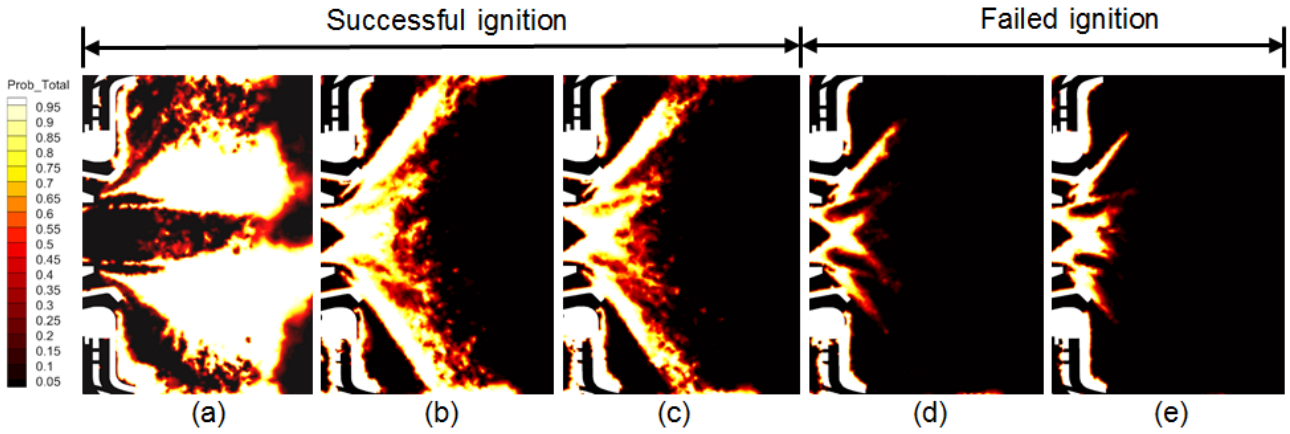

Figure 4 Kernel formation probability calculated with different FARs under TOC1 (a) FAR=0.04, (b) FAR=0.035, (c) FAR=0.031, (d) FAR=0.025, (e) FAR=0.02

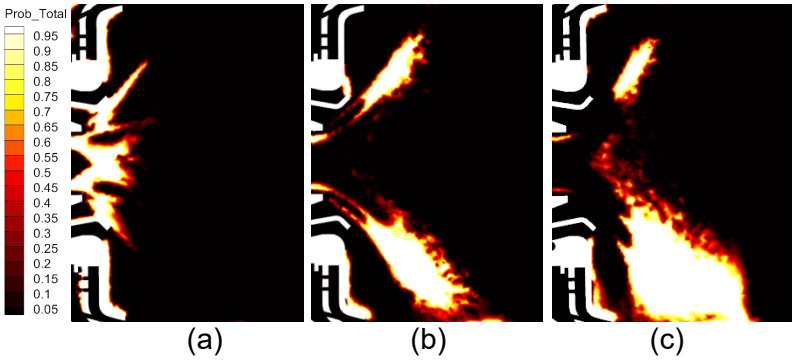

Figure 5 Kernel formation probability predicted with FAR=0.02 under different TOCs (a) TOC1, U_r=5.3m/s, (b) TOC3, U_r=9.4m/s, (c) TOC5, U_r=12.2m/s

4.2 Flame particle evolution

The flame particle tracking results from different FARs and TOCs are plotted in Figure6 and Figure7, respectively. The ignition progress factor π_{Ign} is defined as the volume ratio of cells in burnt state of the primary zone, and $\mathrm{N}_{\mathrm{Active}}$ is the number of active flame particles in the combustor. In present study, the value of critical value $Ka_{p,crit}$ is 1.5 which is recommended by reference [21], and the critical threshold $\pi_{\mathrm{ign,crit}}$ is equal to 0.6. The flame is unable to stabilize in the primary zone with the π_{Ign} less than 0.6. The duration of ignition process can be estimated from these curves as $\mathrm{N}_{\mathrm{Active}}$ reaches zero, and it is evident that ignition lasts within 30ms.

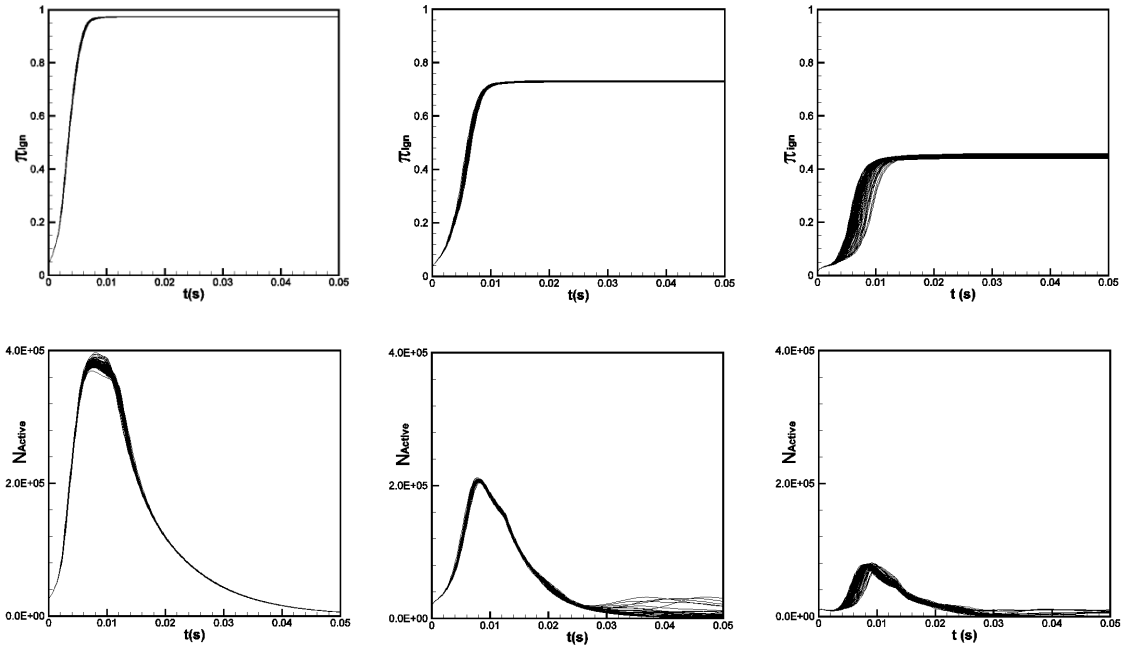

(a) (b) (c)

Figure 6 Evolution of ignition process factor calculated under TOC1 (a) FAR=0.04, (b) FAR=0.031, (c) FAR=0.025

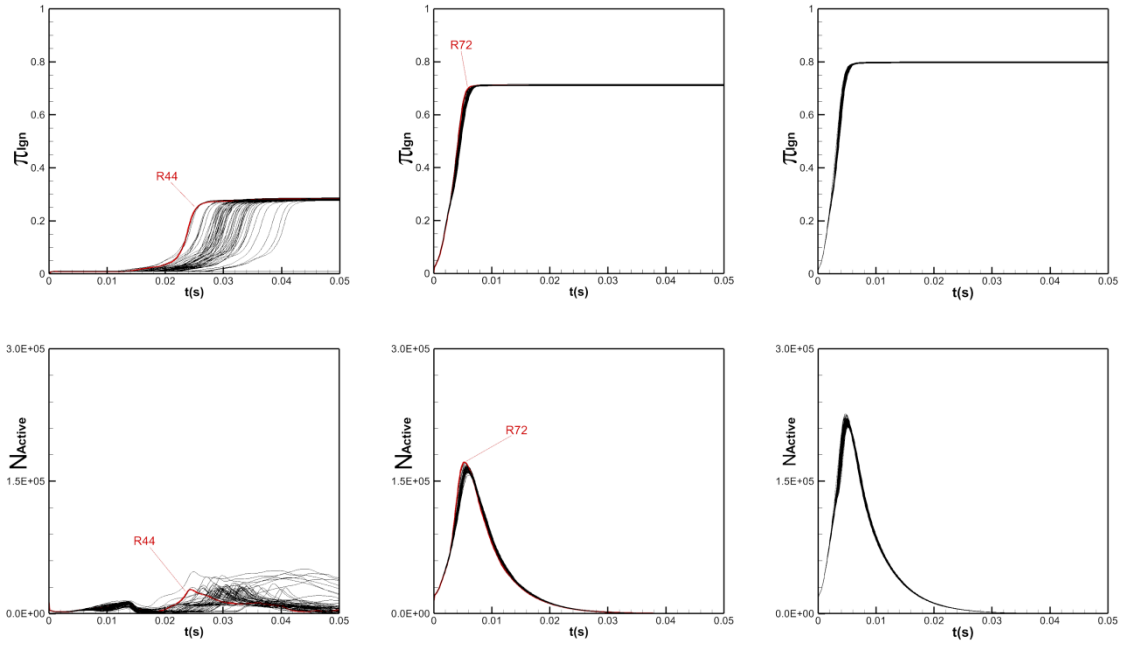

(a) (b) (c)

Figure 7 Evolution of ignition process factor calculated with FAR=0.02 under different TOCs (a) TOC1, U_r=5.3m/s, (b) TOC3, U_r=9.4m/s, (c) TOC5, U_r=12.2m/s

Figure6 shows the effect of FAR on π_{Ign} and $\mathrm{N}_{\mathrm{Active}}$. As the fuel air ratio decreases, both the ignition progress factor and active flame particles decrease. The adverse effect of decreasing FAR on the ignition is evident because of the insufficient fuel to evaporate and the majority of particles with Karlovitz number greater than $Ka_{p,crit}$. As shown in Figure6, the plots in Figure6(a) and (b) indicate the successful ignition while the plots in Figure6(c) indicates the failed ignition. It is noted that the number of active flame particles increase at the beginning of the ignition for all of FARs listed in Figure6. However, in Figure6(c), the volume ratio of cells in burnt state in the primary zone is less than the critical threshold, thus the heat released in the primary zone is insufficient to maintain a stable flame, resulting in failed ignition.

Plots in Figure7 shows the effect of reference velocity on π_{Ign} and $\mathrm{N}_{\mathrm{Active}}$. As shown in Figure7,

both the ignition progress factor and number of active flame particles increase with the reference velocity. These results are consistent with the kernel formation probability distribution shown in Figure5. The mean drop size decrease with the reference velocity, therefore, the increasing fuel vapor concentration leads to lower Karlovitz number which is benefit to the flame propagation.

The 44th spark event in Figure7(a) and 72th spark event in Figure7(b) represent the process of failed ignition and successful ignition, respectively. The evolution of particle and cell states for these two spark events are displayed in Figure8. It is observed that the propagation paths of flame particles are different between failed and successful ignition process. During the period of failed ignition, the flame particles propagate towards to both upstream and downstream of the igniter position. However, these flame particles failed to propagate into the central recirculation zone and the rest of these flame particles propagate towards to the combustor outlet alone the wall surface, resulting in failed ignition of the 44th spark event. On the other hand, the ignition sequence in Figure8(b) shows that the flame particles successfully propagated into the central recirculation zone and trigged plenty of new particles in the primary zone. Therefore, the turbulent flame is full filled in the primary zone resulting in a stable flame in the combustor.

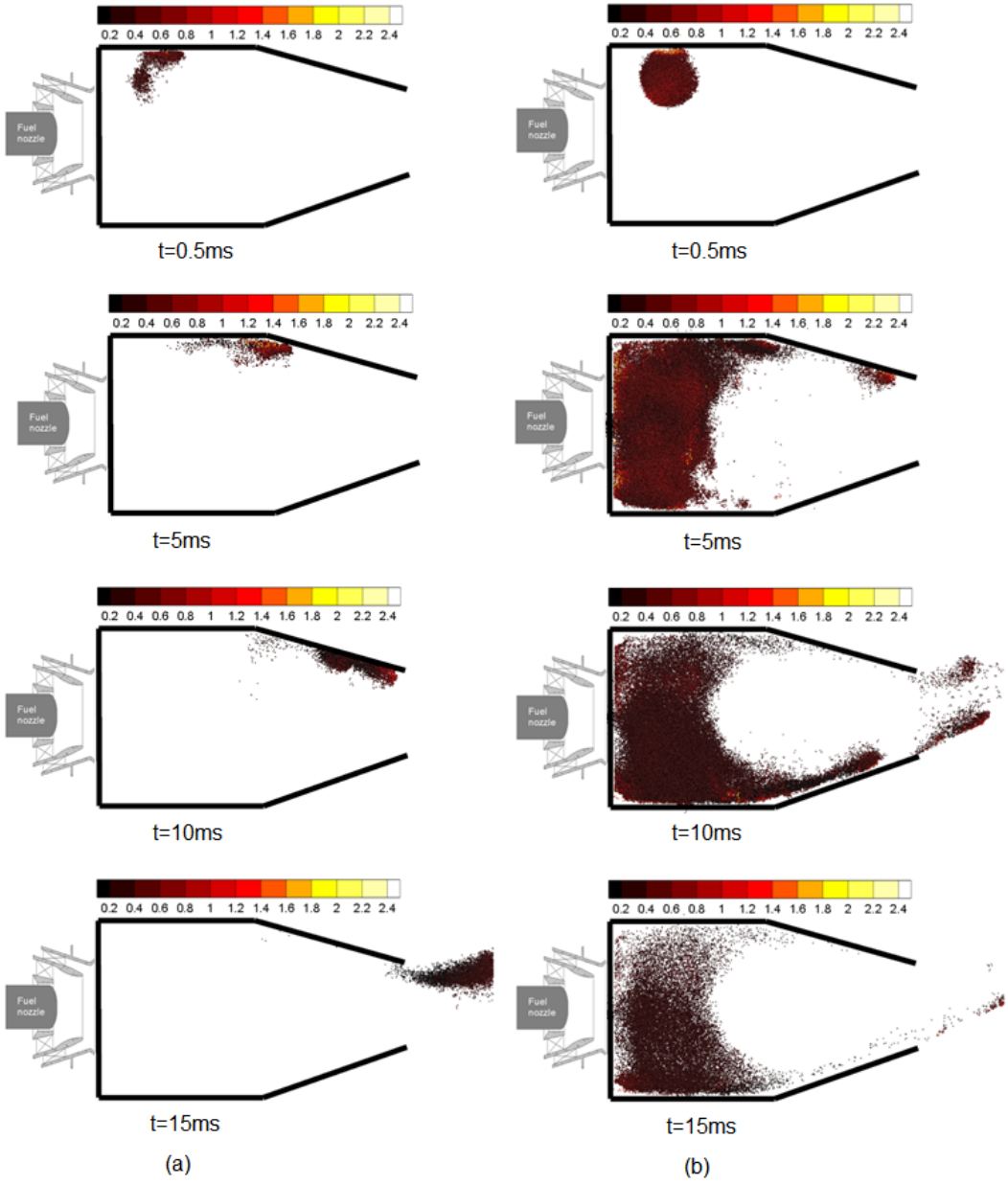

Figure 8 Evolution of particle and cell states for a) 44th spark event under TOC1 with FAR=0.02, b) 72th spark event under TOC3 with FAR=0.02. The particles are colored with particle mixture fraction.

4.3 Ignition probability map

The numerical simulations for ignition are conducted at various spark locations with 100 spark

events at each location. The ignition probability P_{lgn}, mean and variance of π_{ign} are calculated at each spark location. Therefore, the ignition probability map can be obtained and the results are shown in Figure9. It is worth mentioning that the absolute value of $\overline{\pi_{ign}}$ has no physical meaning since it depends on how to specify the domain of interest. However, the light regions with high values of $\overline{\pi_{ign}}$ indicates that the large amount of cells are in burnt state for a given ignition location, resulting in high ignition probability. As shown in Figure 11, the light regions in Figure 11(a), (b) are consistent with the light regions shown in Figure 11(e) and (f).

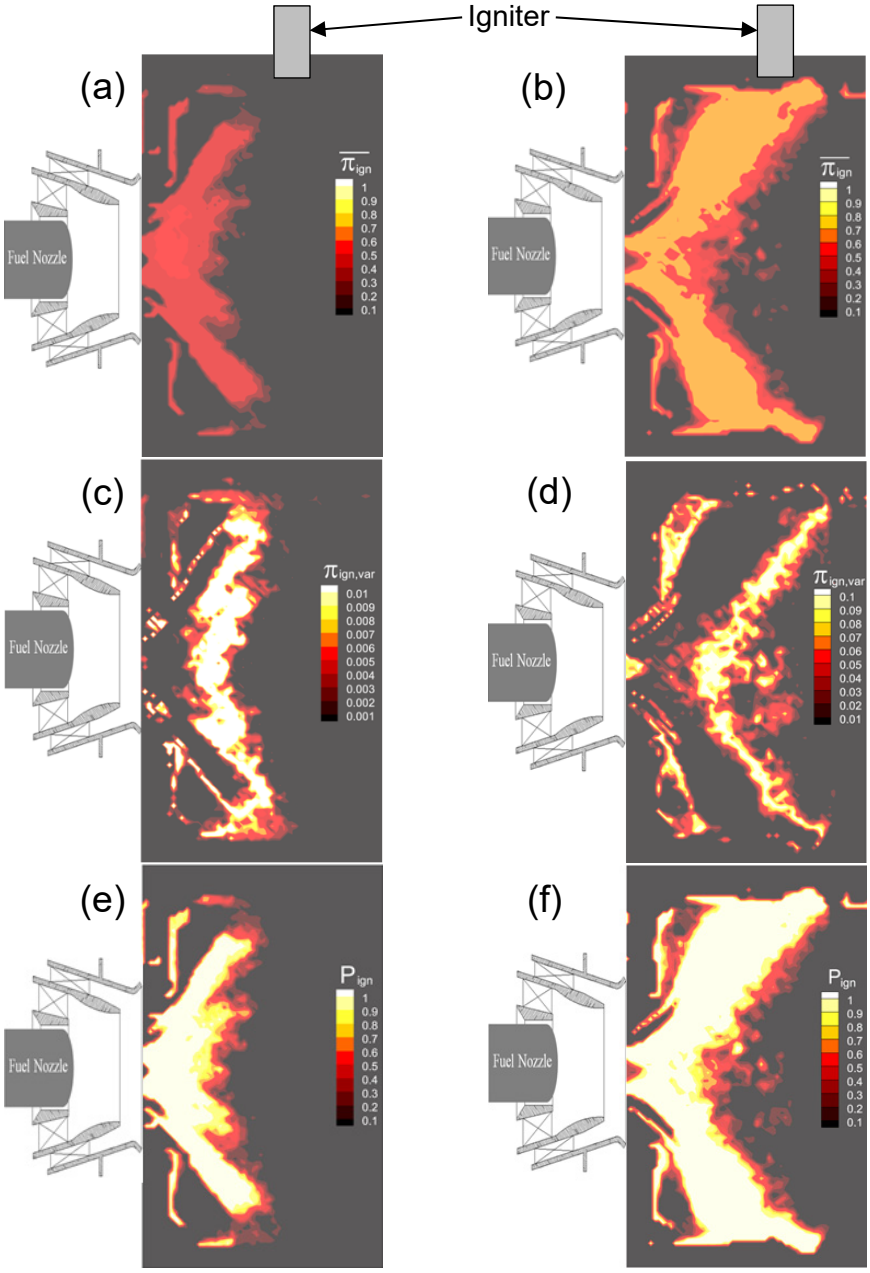

TOC1, *FAR=0.032, U_r*=5.3m/s TOC3, *FAR=0.032,U_r*=9.4m/s

Figure 9 Effect of U_r on the ignition probability map. (a)&(b) mean of π_{ign}, (c)&(d) variance of π_{ign}, (e)&(f) ignition probability.

Figure9(e) and (f) illustrates the best igniter position for the combustor ignition. As shown in Figure9(e), the optimum spark location with the maximum ignition probability is located near the nozzle exit rather than the position of the igniter. It indicates that the original spark location can be optimized for the ignition. However, the practical igniter is always positioned to be level with the outer liner wall for the purpose of preventing igniter erosion. Thus, the optimization of spark location is limited for conventional combustors. As shown in Figure9(f), the highlight with large values of ignition probability expands to the downstream of the igniter. Therefore, the successful ignition can be obtained with the spark released from the original igniter under TOC3.

The effect of reference velocity on the ignition map is also obtained in Figure9 by comparing the

simulation results from TOC1 and TOC3. It is observed that the mean of π_{ign} increases with the reference velocity. It is also noted that the regions with high ignition probability expands as increasing the reference velocity. These results show that the remarkable improvement of ignition performance can be obtained by increasing the reference velocity. The ignition performance improvement is because mean drop size decreases with the reference velocity and mass flow rate. These results also agree well with the experimental results obtained by Naegeli [22].

4.4 Prediction on Lean ignition limits

Figure10 shows the comparisons of ignition limits from experiment and simulation, respectively. The experimental and numerical data in Figure10 are obtained under ground conditions. The solid line in Figure10 is the lean ignition limit obtained from the experiment, while the symbols in Figure10 are derived from the simulation. The colors of the symbols represent the mean ignition progress factor $\overline{\pi_{\mathrm{lgn}}}$ computed by the ignition code. As shown in Figure10, the maximum error of predicted lean ignition limits is less than 5%. It is noted that the successful ignition events are colored with dark red in Figure10, while the failed ignition events are colored with light red. As pointed out in previous section, the critical value of ignition progress factor is 0.6, which is validated by the experimental data as shown in Figure10. However, the critical value of ignition progress factor may vary with the combustor geometries. The effect of the residence time on the lean ignition limit is also illustrated in Figure10, which shows the lean ignition limit increases with the residence time of the combustor.

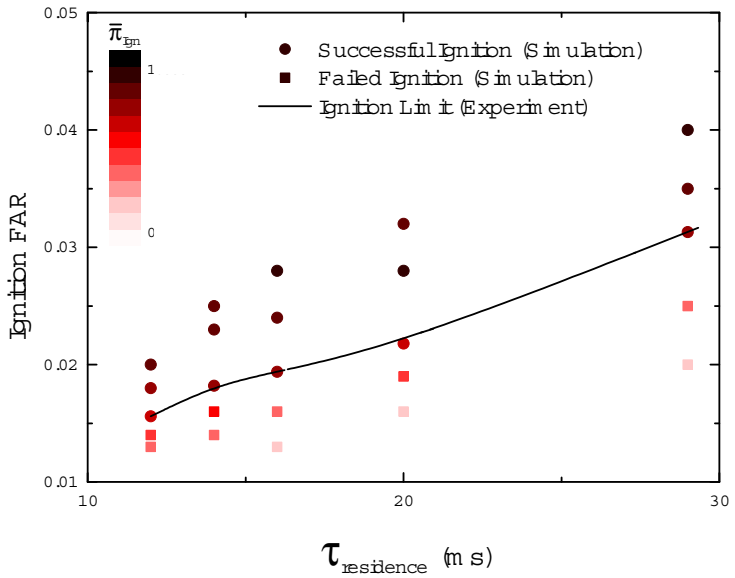

Figure 10 Comparisons between predicted results and measured results for lean ignition limits.

5. Conclusion

In this paper, the hybrid ignition probability analysis has been applied to predict the ignition performance of a gas turbine combustor. This ignition probability analysis method is developed based on the kernel formation criteria coupled with flame particle tracking method. The flame propagation during the ignition process is analyzed with flame particle tracking method in conjunction with the Karlovitz criterion. The kernel formation analysis shows that the ignition performance is related with the kernel formation probability. It is also noted that the droplet profiles and residence time play important roles in both the flame kernel formation and flame particle evolution.

The ignition code is validated with the experimental data from a single dome combustor, and good agreement is obtained between the simulation and experiment. However, the accuracy of the ignition code depends strongly on both the cold CFD simulation, which is input of the ignition models. Therefore, it is necessary to conduct the validations on the cold CFD simulations before implementing the ignition simulation.

In present study, both the kernel formation probability map and ignition probability map are obtained and interpreted for the ignition optimization. The most promising locations for ignition can be determined by both the kernel formation probability map and ignition probability map. The significance of these two maps is roughly equivalent in terms of ignition optimization, while the computational time

of the kernel formation probability map is much less than the ignition probability map.

References

[1] Boileau, M. , et al. "LES of an ignition sequence in a gas turbine engine." Combustion and Flame Vol.154, No.1-2, 2008, pp.2-22.

[2] Choi, Seongman , D. Lee , and J. Park . "Ignition and combustion characteristics of the gas turbine slinger combustor." journal of mechanical science & technology, Vol.22, No.3, 2008, pp:538-544.

[3] Levy Y , Nadvany V , Nehkamkin Y , et al., “Modified Vaporizer for Improved Ignition in Small Jet Engine”. Journal of Propulsion and Power, Vol. 22, No.4, 2006, pp. 828-834.

[4] Goldwasser S R , Saad M A., “Role of pressure in spontaneous ignition”, AIAA Journal, Vol. 7, No. 8, 1969, pp. 1574-1581.

[5] Lefebvre A H., “Fuel effects on gas turbine combustion—ignition, stability, and combustion efficiency”, Vol. 107, No.1, 1985, pp. 24-37.

[6] Ballal D R, Lefebvre A H. “The influence of spark discharge characteristics on minimum ignition energy in flowing gases”, Combustion and Flame, Vol. 24, 1975, pp. 99-108.

[7] Ballal D R, Lefebvre A H. “Ignition and flame quenching of quiescent fuel mists”, Proceedings of the Royal Society of London. A. Mathematical and Physical Sciences, Vol. 364, No.1717, 1978, pp. 277-294.

[8] Peters J E , Mellor A M ., “A spark ignition model for liquid fuel sprays applied to gas turbine engines”, Journal of Energy, Vol. 6, No. 4, 2015, pp. 272-274.

[9] Peters J E , Mellor A M ., “ Liquid fuel spray ignition predictions for JP-10”, Journal of Energy, Vol.7, No.1, 1983, pp. 95-96.

[10]Peters J E , Mellor A M., “Characteristic time ignition model extended to an annular gas turbine combustor”, Journal of Energy, Vol.6, No.6, 1982,pp:439-441.

[11]G. Lacaze, E. Richardson, and T. Poinsot., "Large eddy simulation of spark ignition in a turbulent methane jet", Combustion & Flame, Vol.156, No.10, 2009, pp:1993-2009.

[12]Jones, W. P., & Prasad, V. N., “LES-pdf simulation of a spark ignited turbulent methane jet. Proceedings of the Combustion Institute”, Vol.33, No.1, 2011, pp:1355-1363.

[13]Triantafyllidis A, Mastorakos E , Eggels R L G M., “Large Eddy Simulations of forced ignition of a non-premixed bluff-body methane flame with Conditional Moment Closure”, Combustion and Flame, Vol.156, No.12, 2009, pp:2328-2345.

[14]Subramanian, V., P. Domingo, and L. Vervisch., "Large eddy simulation of forced ignition of an annular bluff-body burner", Combustion and Flame, Vol.157, No.3, 2010, pp:579-601.

[15]Eyssartier A, Cuenot B, Gicquel L Y M, et al., “Using LES to predict ignition sequences and ignition probability of turbulent two-phase flames,” Combustion and Flame, Vol. 160, No. 7, 2013, pp. 1191-1207.

[16]Esclapez, L., Riber, E., & Cuenot, B. “Ignition probability of a partially premixed burner using LES”, Proceedings of the Combustion Institute, Vol.35, No.3, 2015, pp:3133-3141.

[17]Neophytou, A., E. S. Richardson, and E. Mastorakos., Spark ignition of turbulent recirculating non-premixed gas and spray flames: A model for predicting ignition probability, Combustion and Flame, Vol.159, No.4, 2012, pp:1503-1522.

[18]Rizk N, Lefebvre.. “Drop-size distribution characteristics of spill-return atomizersy”. Journal of Propulsion and Power, 1(1)(4), pp. 16–22. 1985

[19]Rizk N K, Mongia H C. Calculation Approach Validation for Airblast Atomizers, Journal of Engineering for Gas Turbines and Power, Vol.114, pp386-394,1992

[20]Ballal D R, Lefebvre A H. FLAME PROPAGATION IN HETEROGENEOUS MIXTURES OF FUEL DROPLETS, FUEL VAPOR AND AIR. Eighteenth Symposium (International) on Combustion, The Combustion Institute, 1981.

[21]T. Soworka, M. Gerendas and R.L.G.M Eggels, NUMERICAL INVESTIGATION OF IGNITION PERFORMANCE OF A LEAN BURN COMBUSTOR AT SUB-ATMOSPHERIC CONDITIONS, Proceedings of ASME Turbo Expo 2014: Turbine Technical Conference and Exposition, 2014.

[22]Naegeli, David W. , and L. G. Dodge. "Ignition Study in a Gas Turbine Combustor." Combustion Science & Technology, Vol.80, No.4-6, 1991, pp:165-184.

Copyright Statement

This work is supported by National Natural Science Foundation of China No.51906234, National Science and Technology Major Project (2017-I-0004-0005) and (2017-I-0003-0003).